BNL-221393-2021-JAAM

Plasma-Initiated Graft Polymerization of Acrylic Acid onto Fluorine-Doped Tin Oxide as a Platform for Immobilization of Water-Oxidation Catalysts

Y. M. Badiei, J. J. Concepcion

To be published in "ACS APPLIED MATERIALS & INTERFACES"

March 2021

Chemistry Department

Brookhaven National Laboratory

U.S. Department of Energy

USDOE Office of Science (SC), Basic Energy Sciences (BES) (SC-22)

DISCLAIMER

Plasma-Initiated Graft Polymerization of Acrylic Acid onto Fluorine-Doped Tin Oxide as a Platform for Immobilization of Water-Oxidation Catalysts

Yosra M. Badiei[*,†] *Christian Traba,*[*,§] *Rina Rosales,*[†] *Anthony Lopez,*[†] *Mohammed Shahid,*[†] *Claudio Amaya,*[†] *Carolina Vera,*[†] *Javier J. Concepcion.*[‖]

[†] Department of Chemistry, Saint Peter's University, Jersey City, NJ 07306, USA

[§]Department of Chemistry, Biochemistry, and Physics, Fairleigh Dickinson University, Teaneck, New Jersey 07666, USA

[‖]Chemistry Division, Brookhaven National Laboratory, Upton, New York 11973-5000, USA

KEYWORDS

FTO, plasma, graft polymerization, acrylic acid, water-oxidation, catalysis, electrochemistry, oxygen-evolution, ruthenium, modified interfaces.

ABSTRACT

The discovery of new and versatile strategies for the immobilization of molecular water-oxidation ($2H_2O \rightarrow O_2 + 4e^- + 4H^+$) catalysts (WOCs) is crucial for developing sustainable and clean energy conversion devices (e.g. (photo)electrocatalytic cells for water splitting). The traditional approach for surface attachment to transparent conductive oxides (e.g. fluoride doped tin oxide (FTO)) is via synthetic modification of the ligand architecture to incorporate functional groups such as carboxylic acids (–COOH) or phosphonates ($–PO_3H_2$) prior to immobilization. However, challenges arising from desorption and the cumbersome derivatizations steps have limited the scope and applications of surface-bound WOCs. Herein, we report for the first time successful immobilization of underivatized Ru(II)-based WOCs (**Ru–Cat1** = $[Ru(tpy)(bpy)(H_2O)]^{2+}$ (tpy = 2,2':6'2''–terpyridine, bpy = 2,2'-bipyridine), **Ru–Cat2** = $[Ru(Mebimpy)(bpy)(H_2O)]^{2+}$ (Mebimpy = 2,6-bis(1-methylbenzimidazol-2-yl) pyridine) and the Ru(II) polypyridyl chromophore **Ru–C3** = $[Ru(bpy)_3]^{2+}$ onto an FTO functionalized plasma-grafted poly(acrylic acid) surface (PAA│FTO). Various characterization techniques such as attenuated total reflectance Fourier transform infrared spectroscopy (ATR-FTIR), scanning electron microscopy (SEM), atomic force microscopy (AFM), and cyclic voltammetry measurements provide evidence for the plasma-induced grafted layer of PAA|FTO and immobilization. Surface stability of the immobilized PAA|FTO and electro-catalytic properties of these new hybrid composite materials were studied at different pH values. Immobilized **Ru–Cat1** and **Ru–Cat2** onto PAA|FTO displayed pH-dependent (Ru^{III}/Ru^{II}) couples and onset catalytic potentials indicative of PCET driven surface reactions. Further findings showed that immobilized WOCs **Ru–Cat1** and **Ru–Cat2** exhibited a higher surface stability in neutral aqueous solutions relative to **Ru–C3.** We attribute this surface stability to the presence of water

ligand in the coordination sphere of immobilized **Ru–Cat1** and **Ru–Cat2** which can H-bond with negatively charged carboxyl groups of the cross-linked grafted PAA polymer brushes. Our findings demonstrate that plasma-grafted polymeric network offers a versatile platform to directly anchor unmodified homogeneous water-oxidation catalysts or chromophores for potential applications in renewable solar-to-fuel energy conversion.

INTRODUCTION

Water-oxidation ($2H_2O \rightarrow O_2 + 4e^- + 4H^+$), one of the half-reactions in water splitting, is a key reaction for the development of an artificial photosynthetic device that aims on a large scale to convert and harness renewable, yet, intermittent energy resources into storable chemical fuels.[1-3] The (photo)electrocatalytic driven water-oxidation reaction forms molecular oxygen and reducing electrons and protons ($4e^-/4H^+$ per 2 mols of H_2O) for the production of clean hydrogen fuel,[4,5] and/or for capture and reduction of carbon dioxide into useful chemical feedstock (Scheme 1).[3]

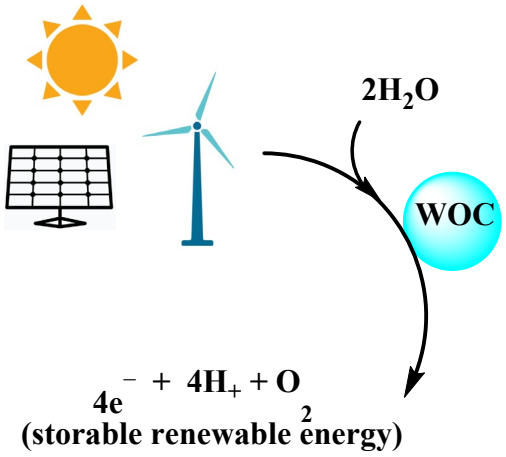

Scheme 1. Sustainable water-oxidation for renewable solar-to-fuel energy conversion.

Water-oxidation is a highly challenging reaction to catalyze as water-oxidation catalysts (WOCs) must be robust under highly oxidizing conditions and produce oxygen at high turnover frequencies (TOF) and low overpotentials beyond the thermodynamic potential ($E^{\circ}_{O_2/H_2O}$ = 1.23 V – 0.059 V × pH vs. NHE).[6,7] Inspired by nature's highly efficient oxygen evolving catalyst, which consists of a $CaMn_4O_x$ (x = 5, 6) tetramer,[8] progress has been made in the last few decades in engineering innovative synthetic WOCs.[9-11] Molecular catalysts are attractive for catalyst design, as their catalytic properties can be fine-tuned by varying the metal core and/or ligand architectures, which can facilitate a better understanding of structure-activity relationships.[7,12] Ever since the discovery of the first molecular WOC, known as the 'blue dimer' $[(bpy)_2(H_2O)Ru^{III}ORu^{III}(OH_2)(bpy)_2]^{4+}$ (bpy = 2,2'-bipyridine) by Meyer and coworkers, numerous molecular catalysts have been reported in recent years.[7,12-14] Impressive O_2 production activities have been recently reached with a number of molecular complexes that are moderately comparable with the reaction rate of 100-400 s^{-1} of the oxygen evolving complex of photosystem II.[15] Typically, optimal efficiencies have been achieved with molecular WOCs based on Ir[16-18] and Ru,[11,19-22] however, some promising examples which incorporate earth-abundant metals such as Co,[23-25] Mn,[10,12] Fe,[26,27] Ni[28,29] and Cu[30,31] have also been shown.

Detailed mechanistic studies have been carried out using single-site homogeneous ruthenium(II) WOCs, such as $[Ru(tpy)(bpy)(H_2O)]^{2+}$ (**Ru–Cat1**) (tpy = 2,2':6'2''–terpyridine; bpy = 2,2'-bipyridine) and $[Ru(Mebimpy)(bpy)(H_2O)]^{2+}$ (**Ru–Cat2**) (Mebimpy = 2,6-bis(1-methylbenzimidazol-2-yl)pyridine.[7,21,32-36] Generally, the criteria for WOCs to accelerate rates of O_2 formation include one or more of the following (i) use of anionic ancillary ligands which

allows access to high-valent intermediates,[34] (ii) incorporating pendent base ligands to facilitate proton-coupled-electron-transfer (PCET) and avoid high energy catalytic pathways,[37] and (iii) addition of basic forms of a buffer (e.g. HPO_4^{2-}, $H_2PO_4^-$, OAc^-) to assist in catalyzing the O–O bond formation step.[38,39]

While progress has been made in elucidating the mechanism of water-oxidation mediated by homogenous molecular WOCs,[6,20,39] for real-world utilization and practical integration in a functional device, employing and interfacing these known molecular catalysts onto conductive solid supports is necessary.[40-42] The immobilization of catalysts on functionalized electrodes offers several advantages for sustainable water-oxidation catalysis over solution-based WOCs. In dye-sensitized photoelectrochemical (DSPEC) devices, immobilizing the WOC and a photosensitizer onto an electrode surface can increase the efficiency of solar driven water-oxidation reactions.[43] In addition, the immobilization of the catalyst can also alleviate the frequently encountered solubility issues of WOCs in aqueous solutions to a great extent, and help create a "heterogenized" recyclable form of well-defined molecular catalytic structures at the electrode interface during the water-oxidation reaction.

Transparent conducting oxides (TCOs) are known for their smart optoelectronic properties and have been extensively utilized as a platform to immobilize molecular water-oxidation, proton or CO_2 reduction catalysts for electrocatalytic fuel-forming reactions.[4,44] A common strategy for the immobilization of Ru-based WOCs onto the surface of TCOs is through the synthetic modification of the molecular catalyst with anchoring functional groups such as –COOH and $–PO(OH)_2$ onto the structure of the ancillary ligand.[4,32,45,46] However, this approach suffers from drawbacks, arising from (a) the synthetic modification of the catalyst which can be costly and

labor intensive and (b) molecular catalyst stability and desorption from the surface due to hydrolysis,[47,48] particularly in neutral and high pH, a regime where the thermodynamic potentials for water oxidation is favorable (E°(NHE) = 1.23 – 0.059V × pH) and faster electro-catalytic rates can be attained.

On the other hand, new strategies for immobilization of WOCs have been recently adopted using a more straightforward approach where the electrode surface is chemically functionalized with nanostructured moieties for molecular attachment onto TCOs. Photochemical grafting of poly(vinylpyridine) on nanostructured indium tin oxide (nanoITO) was utilized to immobilize a cobaloxime hydrogen evolution catalyst.[49] Recently, Meyer and co-workers have demonstrated that nanoITO electrodes can be functionalized with vinyltrimethoxysilane (VTMS) followed by surface electropolymerization of a vinylderivatized complex $[Ru^{II}(Mebimpy)(dvbpy)(OH_2)]^{2+}$ (dvbpy: 5,5′-divinyl-2,2′-bipyridine) which produced a stable surface for water-oxidation between pH 6–7.5.[48] Some of us have shown that self-assembled bilayers (SABs) stabilized via noncovalent interactions of long alkyl chains on a metal oxide can be an anchoring strategy for interfacing Ru WOC catalysts and chromophores to the surface.[50] In the present work, we describe for the first time, the use of the "Grafting-From" approach for plasma-initiated graft polymerization of acrylic acid which contains a terminal carbon-carbon double bonds onto FTO surfaces (Scheme 2). With the "Grafting-From" approach, polymer brush layers can be tailored to possess specific physical and chemical properties of nanostructures.[51-53] The design and construction of plasma-grafted poly(acrylic acid) (PAA) assemblies which contain the negatively charged carboxyl functionality was further studied as a platform for the immobilization of benchmark non-derivatized Ru(II) water-oxidation catalysts **Ru–Cat1** and **Ru–Cat2**, in addition to the Ru(II) polypyridine chromophore **Ru–C3** (Figure 1).

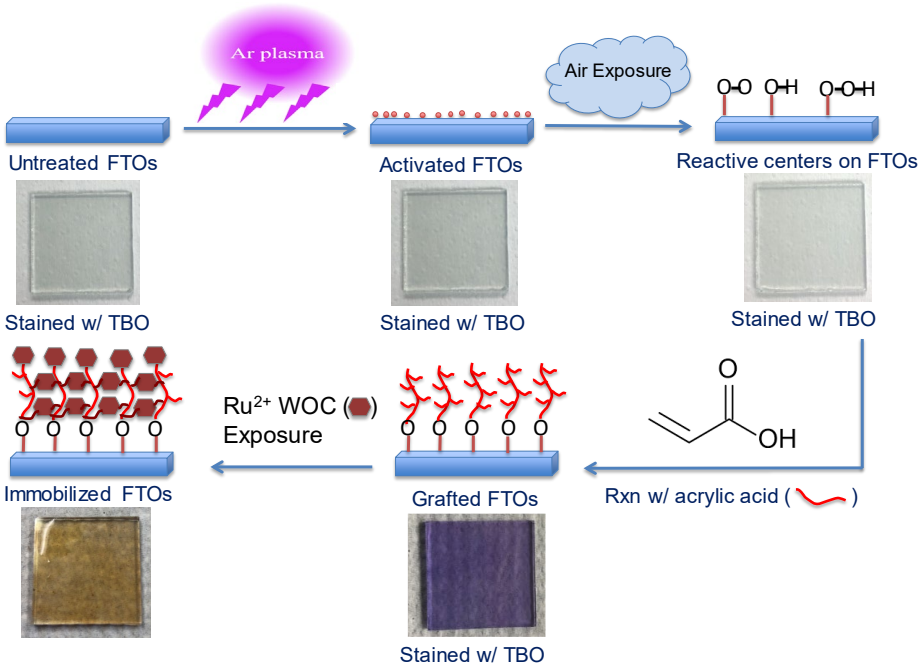

Scheme 2. Schematic diagram of the immobilization process onto plasma-grafted poly(acrylic acid) FTO (PAA|FTO).

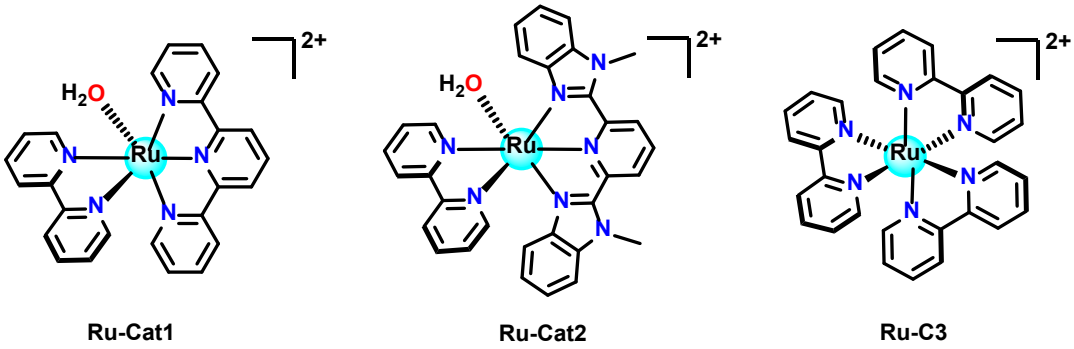

Figure 1. Molecular structures of underivatized Ru(II) WOCs (**Ru–Cat1** and **Ru–Cat2**) and chromophore **Ru–C3** immobilized onto plasma grafted PAA | FTO.

EXPERIMENTAL SECTION

Materials

All solvents and reagents were obtained from commercial sources and used as received unless otherwise noted. Deionized water was obtained using a High Purity Ion Exchange Water System and its conductivity was measured before any experiment (< 20 μS cm^{-1}). Ru(II) complexes: **Ru–Cat1** = $[Ru(tpy)(bpy)(H_2O)]^{2+}$ (tpy = 2,2':6'2''–terpyridine; bpy = 2,2'–bipyridine)[33] and **Ru–Cat2** = $[Ru(Mebimpy)(bpy)(H_2O)]^{2+}$ (Mebimpy = 2,6-bis(1-methylbenzimidazol-2-yl)pyridine) were synthesized according to the literature.[22,54] The **Ru–Cat1** complex was crystallized with the hexafluorophosphate (PF_6^-) counter ion, and for **Ru–Cat2**, the counter ion is triflate (OTf^-). Fluoride doped tin oxide (FTO) glass was purchased from Techinstro (TISXZ 001, sheet resistance 7 Ω sq^{-1}) of dimensions 25mm × 25mm × 2.2mm (thickness) with no passivation layer. The FTO coated glass plates were stored in concentrated sulfuric acid for 24 hours before use and rinsed with distilled water and sonicated in ethanol for 10-15 mins before grafting.

Generation of gas discharge plasma.

Argon discharge gas was produced using a Plasma Prep III device (SPI Supplies, West Chester, PA, USA). This plasma device is operated under vacuum and contains a reactor comprising a Pyrex glass chamber (10.45 cm in diameter) and a pair of electrodes (an upper and lower electrode). A radio frequency generator was supplied with a frequency of 13.56 MHz and had an output of up to 100 W. The system was evacuated to 300 mtorr and argon gas was introduced to the chamber at a flow rate of 0.068 $m^3\ h^{-1}$. Bottled argon was purchased from Praxair (Keasbey, NJ, USA) and was prepared by cryogenic air separation, which led to a purity of >99.9%. The

chamber pressure was maintained at 360 mtorr.[51,52] The plasma treatment was conducted on the FTO conductive film side of the planar electrode and the electrodes were placed approximately 8 cm away from the discharge gas outlet. Exposure of FTOs to argon plasma is essential for the graft polymerization reaction and is described in detail under the Results and Discussion section.

Preparation of Ru(II) immobilized PAA │FTO electrodes.

Ruthenium(II) complexes (**Ru–Cat1** and **Ru–Cat2**) were immobilized onto the poly(acrylic acid) grafted FTO films (PAA │FTO) by submerging the grafted FTO slides in an aqueous solution containing 1.0 mM of the Ru catalyst containing 10% (v/v) of 2,2,2-trifluoroethanol (TFE) as a co-solvent to enhance the catalyst solubility, for 1–4 hours. For the **Ru–Cat2** and **Ru–C3**, the grafted slides were soaked overnight in a 1.0 mM aqueous solution of the Ru(II) complex. The immobilized slides were then thoroughly washed with deionized water to remove any unbound Ru complex and finally air-dried prior to any characterization or electrochemical measurements.

Physiochemical characterization of grafted films

Argon plasma treated, grafted, and PAA │FTO electrodes were characterized using attenuated total reflectance Fourier transform infrared spectroscopy (ATR-FTIR) (JASCO FT/IR-460Plus), Toluidine Blue-O (TBO) staining, and visualized using Scanning Electron Microscopy (SEM) and Atomic Force Microscopy (AFM). ATR-FTIR was conducted in the percent transmittance mode in the range of 400–4000 cm^{-1} with a KRS-5 prism and an incident angle of 45°. The graft density on grafted FTOs was determined by a colorimetric method using Toluidine Blue-O staining, assuming the molar ratio between carboxyl groups and the dye to be unity.[51,52] A 0.5

mm dye solution was prepared at a pH of 10 and grafted FTOs were placed in this solution for 6 hours at 30 °C. The FTOs were then removed and thoroughly washed with sodium hydroxide solution of pH 9 to remove any non-complexed dye adhering to the surface. The dye was desorbed from the FTOs in 50% acetic acid aqueous solution and the final dye content was obtained by measuring the optical density of the solution at 633 nm using a UV-visible spectrophotometer. SEM images were obtained using an Auriga scanning electron microscope. SEM images of FTOs, including control (argon plasma treated), grafted, and immobilized FTOs were taken, coated with gold for 30 seconds and then attached to the SEM stage using conductive tape for imaging. The applied voltage was 2 kV. AFM measurements of FTOs, including control (argon plasma treated), grafted, and PAA│FTO were taken in air on an NSCRIPTOR dip pen nanolithography system (Pacific Nanotechnology, Inc.) using P-MAN-SICC-0 AFM cantilevers with a nominal force constant of 40 N/m in tapping mode.

Electrochemical Measurements.

Electrochemical experiments were conducted using a CHI630E electrochemical workstation (CH Instruments, Inc., Austin, TX, USA). An electrochemical cell is realized by employing (FTO, PAA|FTO or the Ru complex immobilized on PAA│FTO) as the working electrode, a Pt wire counter electrode, a Ag/AgCl aqueous reference electrode (sat. KCl(aq), 0.198 V vs. NHE). The potential of the Ag/AgCl reference electrode in electrochemical experiments was constantly checked before and after electrochemical experiments and small drift in the electrodes potential of < 5 mV were found. A copper tape was attached to the modified FTO electrode and half of the surface area of the slide was exposed to the electrolyte and the unexposed area of the electrode was masked by a Teflon tape. For the stability protocol, a series of CV scans (4-8 segments)

from 0.0 – 1.2 V vs. Ag/AgCl; scan rate 100 mV s^{-1} were done to equilibrate the slide prior to recording the initial voltammogram. The surface coverage of the immobilized complex, Γ in mol/cm^2, were determined from CV measurements according to equation 1 where $Q_{Ep,a}$ is the integrated charge for the anodic wave, n is the number of electrons transferred per redox site (moles e−), F is the Faraday constant (96,485 C/mol), A is the area of the half of the immobilized electrode (3.125 cm^2). The stability of immobilized Ru(II) WOCs **Ru–Cat1** and **Ru–Cat2**, and chromophore **Ru–C3** on PAA|FTO were evaluated by monitoring the Ru^{III}/Ru^{II} peak current vs. time using cyclic voltammetry as shown in the supporting information. The surface coverage values of the immobilized grafted electrodes are summarized in Table S1 in the supporting information.

$$\Gamma = \frac{Q_{E_{p,a}}}{n\mathrm{FA}} \qquad (1)$$

RESULTS AND DISCUSSIONS

Construction of plasma-induced grafted PAA assemblies on FTO (PAA │FTO)

Plasma technology has been utilized as an effective tool for the functionalization of polymeric material or synthesis of nanomaterials on transparent metal oxide films such as TiO_2[55] and introduce desirable functional properties.[51-53,56,57] Plasma-modified FTO counter electrodes with cobalt selenide nanomaterials have been shown to improve the performance in dye-sensitized solar cells (DSCC).[58] This has been attributed to the increase in surface hydrophilicity, nanoparticle packing density, higher dye loading, and improved electron transport and reduced recombination. Moreover, a polymer can be grafted onto a plasma-activated surface from a desired monomer resulting in self-assembled polymer nanostructures on the surface. Some of us have previously reported the use of argon plasma-initiated grafting technology for the

construction of polymer brushes on biomaterial surfaces.[51-53] In this work, plasma-induced surface polymerization of FTO, using acrylic acid as a monomer which contains a terminal carbon-carbon double bonds has been carried out as shown Scheme 2. The plasma-initiated graft polymerization technique has a chemically different mechanism in comparison to conventional polymerization techniques. This uniqueness stems from a free-radical polymerization reaction, which is initiated at the surface of the material.[51-53] In the "Grafting-From" approach, inelastic collisions between the electrons, radicals and neutral atomic species found in the plasma create reactive radical centers on the surface. These radicals initiate the free-radical polymerization reaction when the appropriate experimental conditions are met.

Exposure of FTOs to the argon plasma was evaluated under two experimental parameters: 1) argon plasma power and 2) argon plasma exposure time (Figure 2). In the second step, the activated surfaces are then exposed to air to generate hydroperoxide, hydroxyl, and peroxide reactive centers (Figure 2).[51-53] After exposure to air, the activated FTOs are then placed into acrylic acid monomer solutions of a specified concentration. The graft polymerization reaction of acrylic acid was carried out at 70 °C, under a nitrogen atmosphere for 8 hours, which initiates the free-radical surface grafting mechanism at the reactive centers (Scheme 1). Notably, this plasma-assisted surface grafted approach described here can also be applied to other surfaces such as carbon nanoparticles, TiO_2 or PET.[51-53]

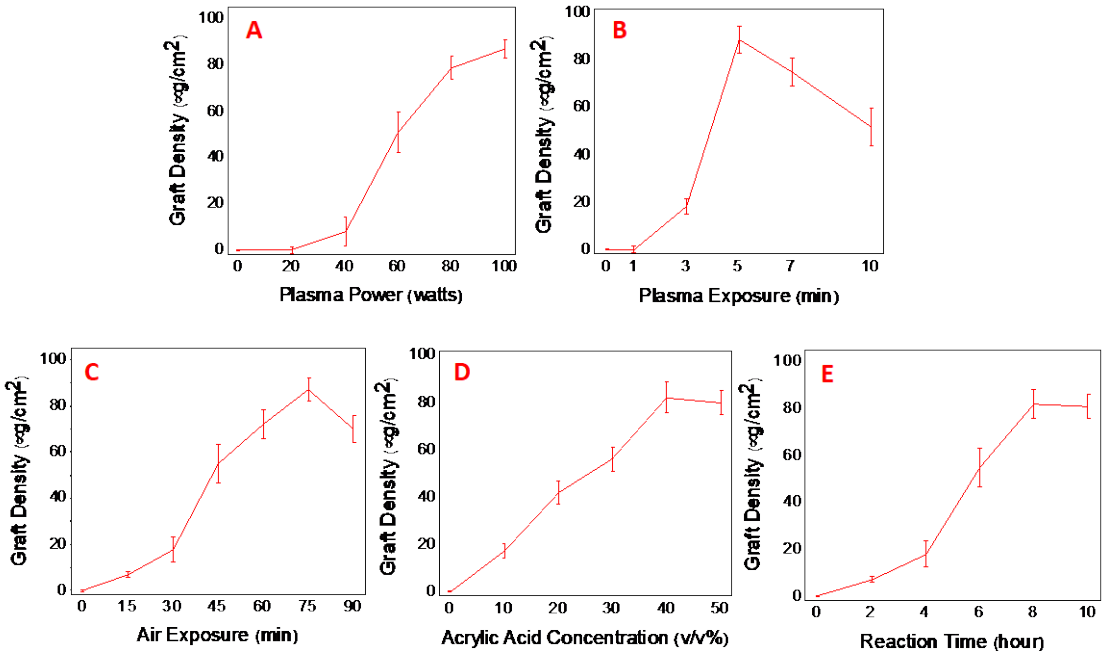

Figure 2. Grafting density on FTOs as a function of: 1) discharge power (A), with argon plasma, 5 min exposure time, 75 min air exposure, 8 hours of reaction time, and monomer concentration of 40% (v/v); 2) plasma exposure time (B), with argon plasma, 100 watts discharge power, 75 min air exposure, 8 hours of reaction time, and monomer concentration of 40% (v/v); 3) air exposure time (C), with argon plasma, 100 watts discharge power, 5 min exposure time, 8 hours of reaction time, monomer concentration of 40% (v/v); 4) monomer concentration (D), with argon plasma, 100 watts discharge power, 5 min exposure time, 8 hours of reaction time, and 75 min air exposure; 5) and reaction time (E), with argon plasma, 100 watts discharge power, 5 min exposure time, and 75 min air exposure and monomer concentration of 40% (v/v), were all studied and each of the experimental conditions affected poly(acrylic acid) grafting on nanoparticles. The amount of PAA grafting content was calculated using Toluidine Blue O staining assay. Data represent the mean and SD of twenty samples.

Plasma optimization of surface grafted FTOs

The plasmas generated in our lab are "non-thermal plasmas". Non-thermal plasmas are formed because the electrons within the plasma possess much higher temperatures and consequently higher energies than those of the ions and the neutral species.[59] These plasmas typically have temperatures between 40–100 degrees Celsius. The advantages of using cool plasmas generated at atmospheric pressure are that (1) the thermal load on the material is negligible and (2) the reactive species in the argon plasma are gentle enough that surface modification is confined to a depth of just a few nanometers and only the surface of the material is modified.[51-53,59] During the optimization process, experimental conditions including: (1) argon plasma power; (2) plasma treatment time; (3) exposure time to air; (4) reaction time with monomer solutions; and (5) concentration of monomer solutions, were studied and were found to effect the graft density and the polymer brush length of the grafted materials.[51,52] It is known that plasma power, treatment time, and exposure to air, all effect brush density, while reaction time with the monomer solution and monomer concentration, both effect brush length.[51,52] Throughout the optimization process, the formation of surface hydroperoxide, hydroxyl, and peroxide reactive centers were uniformly present on FTOs and were studied using the TBO assay (Scheme 2). The amounts of hydroperoxide, hydroxyl, and peroxide reactive centers generated onto a surface initiate the "Grafting-From" modification technique, and are directly proportional to the graft density.[51,52] In agreement with other studies, plasma discharge powers positively affected surface activation, with significant amount of hydroperoxides, hydroxyls, and peroxides being generated at discharge powers as low as 60 W, when plasma treatment times, air exposure times, monomer solution concentrations, as well as reaction times were kept constant (Figure 2A). Unlike the other studies, increasing discharge powers to 100 W had significant effects on graft content, with

a maximum graft density of 84 μg/cm^2 for FTOs. When discharge power was fixed at 100 W, the optimal argon plasma treatment time was determined to be 5 minutes (Figure 2B). This disparity between discharge powers is a direct result of the different chemical composition of the surfaces being used. Extended or shortened plasma exposure times led to lower graft content and followed a bi-phasic trend for both the modification of FTOs (Figure 2B). Interestingly, there was also a very similar bi-phasic trend with respect to air exposure times for FTOs (Figure 2C). When plasma treatment time, monomer solution concentrations, and discharge power were fixed, the optimal exposure time to air for FTOs was 75 min, respectively (Figure 2C). Similarly, as with other studies, an increase in the concentration of monomer solutions positively affected the graft content (Figure 2D). In fact, as monomer concentrations increased, so did the graft density. However, as monomer concentrations reached more than 40% (v/v), limited increases in the graft content of FTOs was observed, as a result of self-polymerization in the monomer solution.[51,52] As previously seen, the effects from extended reaction time with monomer solutions had a positive correlation and played a significant role on the lengths of polymer brushes when plasma treatment time, discharge power, air exposure time, and monomer solution concentrations were fixed (Figure 2E). However, limited brush thickness increases were negligible after 8 hours of reaction time (Figure 2E). Optimized experimental conditions for the plasma-mediated surface modification was in agreement with other published trends and could easily be controlled by manipulating surface activation experimental conditions.[53]

Immobilization of underivatized Ru(II) WOCs on plasma grafted PAA │FTO

The strategy of direct immobilization of underivatized molecular water-oxidation catalysts onto the surface of optimized plasma grafted PAA │FTO films was further applied. We have chosen

to graft PAA onto FTO surfaces as it consists of negatively charged carboxylate sites per chain (pK_a of AA = 4.2) which can electrostatically bind with the positively charged Ru(II) catalysts in aqueous solutions as shown in Scheme 2. The immobilization of molecular catalysts onto a polymer-grafted electrodes to make hybrid constructs has several advantageous, (1) provides a scaffold to incorporate a variety of catalysts without the need for synthetic modification, (2) can lead to a higher surface loading of the catalyst per unit area, (3) polymer linkers can provide mechanical and chemical stability for the attached molecules and optimize the catalytic performance by facilitating charge transfer to redox-active sites.[60,61]

Upon immersing PAA│FTO in an aqueous solution containing 1.0 mM aqueous solution of the Ru(II) water-oxidation catalyst (**Ru–Cat 1)**, immobilization immediately occurred. By visual inspection, the modified FTO electrodes exhibited a pale orange color indicating the presence of the immobilized catalyst on the grafted FTO within few minutes. After a given period of incubation (~4 hours), the **Ru–Cat1**│PAA│FTO slide was copiously washed with deionized water and ethanol to eliminate unwanted absorbed molecules or deposits from the film. We further examined our PAA grafting approach to immobilize other non-derivatized ruthenium complexes, such as the molecular water-oxidation catalyst, **Ru–Cat2** = $[Ru(Mebimpy)(bpy)(H_2O)]^{2+}$ (Mebimpy is 2,6-bis(1-methylbenzimidazol-2yl; bpy = 2,2' bipyridine), and the well-known photochemical oxidant **Ru–C3** = $[Ru(bpy)_3]^{2+}$. Plasma grafted PAA|FTO slides displayed a pale orange and yellow color films after submerging the samples in 1 mM **Ru–Cat2** and **Ru–C3** complex solutions overnight respectively. Each step of the immobilization process was studied using electrochemical methods, the TBO staining method, ATR-FTIR, AFM and SEM as discussed in the below sections.

Electrochemical Characterization

To ensure that the Ru(II) complexes were immobilized on the grafted PAA|FTO electrode surface, electrochemical measurements was initially performed below the thermodynamic OER (OER = oxygen evolution reaction, $E°$(NHE) = 1.23 – 0.059V × pH). The cyclic voltammetry (CV) of **Ru–Cat1**│PAA│FTO showed a distinct reversible redox wave at $E_{1/2}$ ~ 0.60 V vs. Ag/AgCl in 1.0 M KNO_3 aqueous solution characteristic of the successful immobilization of **Ru–Cat1** complex (Figure 3). A small peak-to-peak separation at this potential ($\Delta E_p = E_{p,a} - E_{p,c}$) ≤ 30 mV was recorded for all CVs displaying a signal shape diagnostic of a redox species tethered to the surface of an electrode. A linear relationship between the peak current and the scan rate was obtained and is consistent with a surface couple (Figure 4). This indicates that the heterogeneous electron-transfer (ET) reaction between the bound **Ru–Cat 1** molecule and the surface-grafted polymer film is rate-limiting, and that the rate of ET is not determined by a freely diffusing species.[62] Furthermore, the anodic and cathodic peak currents measured from repeated CVs are almost equivalent suggesting that the immobilized **Ru–Cat1** complex can be completely oxidized and reduced under these conditions. This reversibility also indicates that a constant number of immobilized Ru(II) electroactive centers attached to the surface can be interconverted between the oxidized and reduced states. Furthermore, under optimal experimental conditions, surface coverages of the **Ru–Cat1**│PAA│FTO, Γ, as estimated from the integrated charge passed under the anodic peak reach 1(±0.5) × 10^{-9} mol/cm^2 of the geometric area of the FTO electrode upon soaking the slides for a duration of 4 h, and is comparable to previous work on surface-bound Ru(II) polypyridyl complexes.[48] Non-plasma treated bare FTO control slides soaked in a 1.0 mM solution of **Ru–Cat1** for the same duration (4 h) did not exhibit any redox

peaks on the surface as shown in Figure 3. In conclusion, this confirms that the plasma-grafted polymeric PAA coating is necessary for anchoring the catalyst to the FTO electrode.

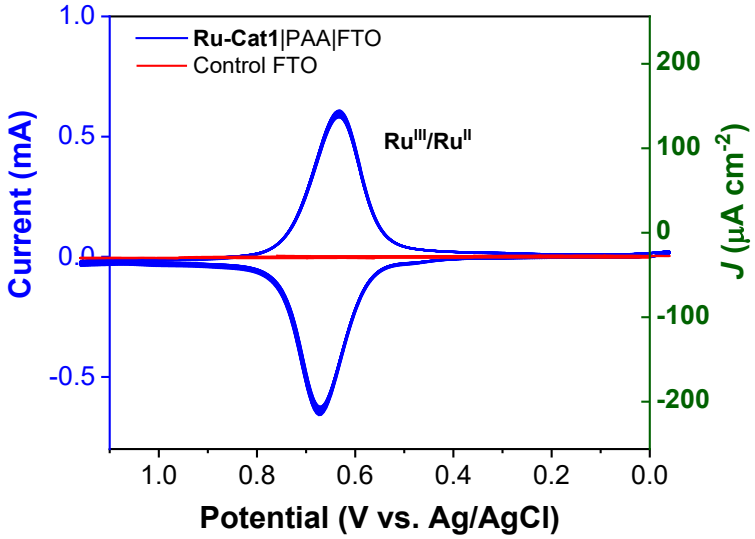

Figure 3. Cyclic voltammograms (CVs) of immobilized **Ru–Cat1**|PAA|FTO (blue) upon performing 50 consecutive scans from 0 to 1.2 V vs. Ag/AgCl and control bare FTO electrode (red). The measurements were performed in aqueous 1.0 M KNO_3 at a scan rate of 0.1 V/s.

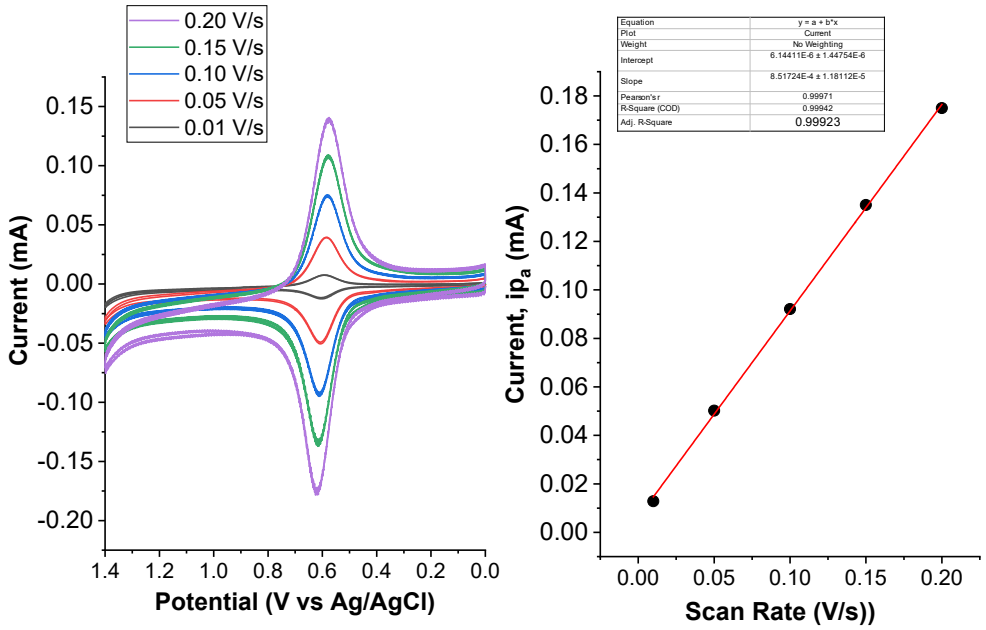

Figure 4. Left: cyclic voltammograms recorded of **Ru–Cat1**|PAA|FTO grafted electrode at various scan rates decreasing from 0.2 V/s to 0.01 V/s in 1.0 M KNO_3. Right: Linear scan-rate dependence on anodic current peak.

Furthermore, the chemical stability of immobilized **Ru–Cat1** | PAA | FTO electrode was investigated in aqueous solutions. Upon sweeping the oxidation potential from 0 to 1.2 V vs Ag/AgCl and upon performing multiple consecutive scans (25-100 cycles, scan rate = 0.1 V/s) in an aqueous containing 1.0 M KNO_3, no discernible change in the redox peak currents was observed (Figure 3; Figure S1). Time-dependent studies followed by monitoring the CV over the course of three hours recorded in 1.0 M KNO_3 electrolyte showed stable voltammograms (Figure S2) and no leaching of the surface-bound complex. When the modified electrode was stored dry, no decrease in the electrochemical signal was observed when analogous experiments were conducted over several consecutive days. This firmly indicates the high chemical stability of the

immobilized **Ru–Cat1**|PAA│FTO film under these conditions and the chemical robustness of the grafted PAA layer under an electrochemically oxidative environment. Oxidatively induced surface coverage loss to about 82% has been reported before with a phosphonate-derivatized Ru(II) polypyridine complex.[63] We believe that the improved stability and robustness of our modified **Ru–Cat1**│PAA│FTO surface in aqueous solutions is due to the presence of the multiple attachment sites (carboxyl groups) between the PAA polymer brushes and **Ru–Cat1** which stabilizes catalyst surface binding and prevents desorption under these conditions (see Scheme S1). The formation of cross-linked polymer network ensued from cross reactions between grafted chains and brushes entanglement, due to hydrogen bonding between carboxylic groups and water, is also likely to re-enforce catalyst binding to the platform surface (see Scheme S2). Some of us have reported similar findings in studies with Ag immobilized nanoparticles on plasma-induced grafted polymerization of PET films.[51-53]

Figure 4 displays the CV of bare FTO in a 1 mM homogeneous **Ru–Cat1** in 0.1 M phosphate buffer (pH 7) in comparison to the immobilized **Ru–Cat1|PAA|FTO** electrode. In solution, **Ru–Cat1** exhibits two quasi-reversible waves assigned in accordance to its Pourbaix diagram as $[Ru^{III}–OH]^{2+}/[Ru^{II}–OH_2]^{2+}$ ($E_{1/2}$ = 0.55 V vs. Ag/AgCl) and $[Ru^{IV}=O]^{2+}/[Ru^{III}–OH]^{2+}$ ($E_{1/2}$ = 0.70 V vs. Ag/AgCl) respectively with a narrow potential gap between the Ru(IV/III) and the Ru(III/II) couples ($\Delta E_{1/2}$ = ~ 0.15 V) followed by the $[Ru^{V}=O]/[Ru^{IV}=O]$ ($E_{1/2}$ = 1.4 V vs. Ag/AgCl) that precedes the catalytic water-oxidation current wave. In contrast, the CV of the immobilized **Ru–Cat1**│PAA│FTO shows a coalesced reversible redox wave at $E_{1/2}$ = 0.60 V vs. Ag/AgCl prior to the catalytic wave at 1.4 V vs. Ag/AgCl. This single-wave observed with immobilized **Ru–Cat1** may be assigned to the Ru(III/II) redox couple as it closely resembles the potential value of the first-wave of the catalyst in solution. The second-redox event

(Ru^{IV}=O/Ru^{III}–OH_2 couple) was not evident as it can be coalesced with the first surface peak due to the narrow potential gap between them or it can be kinetically inhibited as reported before with immobilized Ru(II) carboxylate WOCs containing phosphonic acid linkages. [37,45]

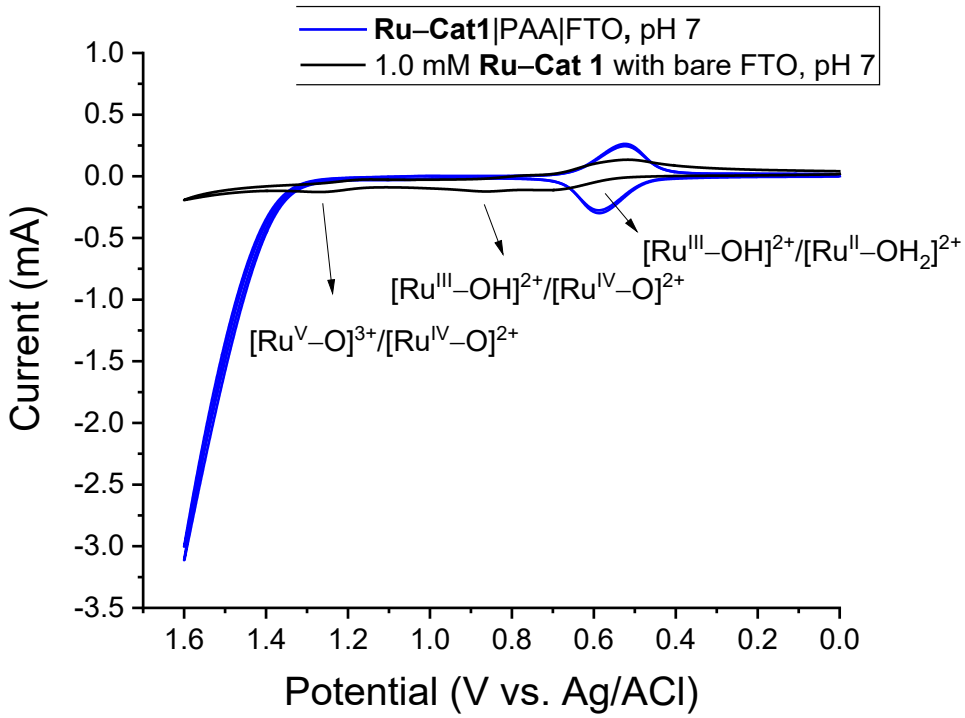

Figure 5. Comparison of cyclic voltammogram (CV) of a 1.0 mM solution of **Ru–Cat1** = $[Ru(tpy)(bpy)(H_2O)]^{2+}$ prepared in 0.1 M phosphate buffer adjusted to pH 7 with bare FTO (black), and the CV of surface immobilized **Ru–Cat1**|PAA|FTO (blue). The measurements were performed by scanning 4 consecutive segments from 0 V to 1.6 V vs. Ag/AgCl at a scan rate of 0.1 V/s.

We further embarked on immobilizing other non-derivatized Ru(II) molecular complexes onto the plasma grafted PAA|FTO. The comparative CVs of immobilized **Ru–Cat1**, **Ru–Cat2** and

Ru–C3 on the grafted surface in an aqueous 1.0 M KNO_3 electrolyte are shown in Figure S3. Similar to the anchored **Ru–Cat1**, a linear plot of the oxidation peak current (i_{pa}) for the Ru^{III}/Ru^{II} wave ($E_{Ru^{III}/Ru^{II}}$ = 0.5 V vs. Ag/AgCl) and the scan rate (υ) was obtained for **Ru–Cat2**|PAA|FTO (Figure 6). This is consistent with a surface-coupled redox and the successful integration of non-derivatized **Ru–Cat2** on the grafted polymeric film. The calculated surface coverage from the integrated charge of the anodic Ru(III/II) surface wave for the immobilized **Ru–Cat2** and **Ru–C3** are $\Gamma = 7.8(\pm0.3) \times 10^{-10}$ mol/cm^2 and $\Gamma = 2(\pm0.5) \times 10^{-11}$ mol/cm^2 respectively; as shown in Table S1. Interestingly, in the case of immobilized **Ru–Cat2**, another apparent peak in 1.0 M KNO_3 was observed due to the surface couple $[Ru^{IV}{=}O]^{2+}/[Ru^{III}{-}OH]^{2+}$ ($E_{Ru^{IV}/Ru^{III}}$ = 0.7 V vs. Ag/AgCl) between scan rates 0.2 V/s to 0.05 V/s, albeit this second wave appears more diminished as compared to the first wave (Figure 6). The observation the second surface-wave which we assign as $[Ru^{IV}{=}O]^{2+}/[Ru^{III}{-}OH]^{2+}$ in the case of immobilized **Ru–Cat2**|PAA|FTO indicates that the grafted polymeric film does not inhibit the formation of high valent Ru intermediates on the surface. Background subtracted electrocatalytic currents of immobilized **Ru–Cat2**|PAA|FTO show a decrease in the onset-potential and increase in catalytic current when the pH was increased from 4.5 to pH 8 (Figure S4, Table S2). This is consistent with the base-assisted catalytic PCET process as previously reported in solution. In contrast, the surface integrated Ru(II) chromophore **Ru–C3** shows a lower loading and binding to the grafted PAA film as compared with **Ru–Cat1 and Ru–Cat2** (Figure S3, Table S1). After repeated consecutive CV scans at low pH (pH ~5) in 0.1 phosphate buffer a more stable $Ru^{III/II}$ peak current signal identified at 1.05 V vs. Ag/AgCl for the **Ru–C3**|PAA|FTO film was obtained, albeit with a low equilibrium surface coverage ($\Gamma = 1.5 \times$

10^{-11} mol cm^{-2}) (Figure S5). Noticeably, the Ru^{III}/Ru^{II} surface redox wave for the immobilized **Ru–C3** films rapidly decreased in 0.1 M phosphate buffer when the pH was adjusted from low pH ~ 4 to more a basic pH 7.5, and the color of the solution turned yellow due the desorption of the complex from the surface (Figure S6). We believe that the higher catalyst loading and superior electrochemical stability in neutral aqueous solutions of the surface catalysts (**Ru–Cat1** and **Ru–Cat2)** in comparison to the **Ru–C3** grafted onto PAA|FTO is attributed to the presence of the water ligand in the coordination sphere. H–bonding between the aqua ligand and the carboxylic group ($RCOO^-$) of the grafted polymeric chains of the PAA film can favorably enhance the binding to the surface (Scheme S2).

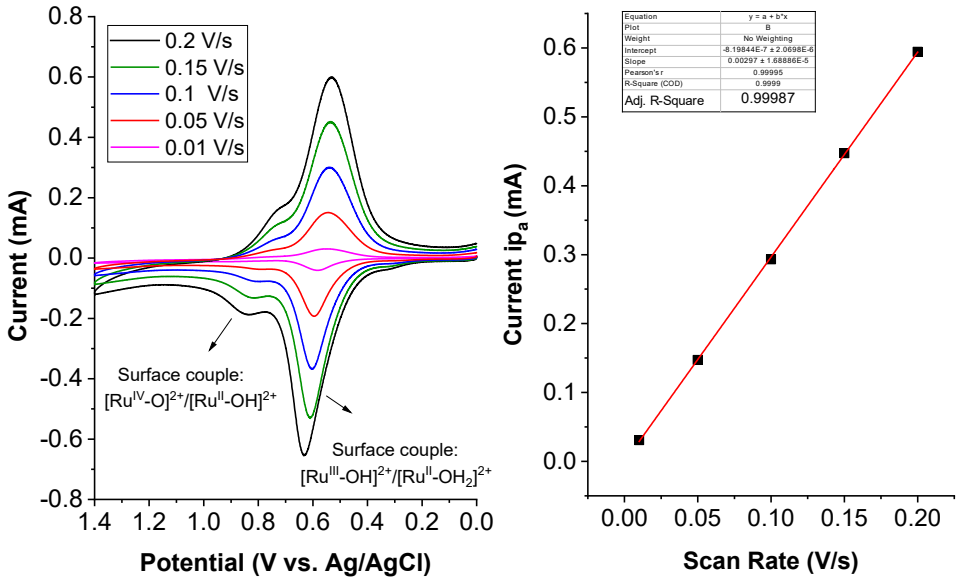

Figure 6. Left: cyclic voltammograms recorded of **Ru–Cat2**|PAA|FTO grafted electrode at various scan rates decreasing from 0.2 V/s to 0.01 V/s in in an aqueous solution of 1.0 M KNO_3. Right: Linear scan-rate dependence on anodic current peak for immobilized **Ru–Cat2**|PAA|FTO.

IR Characterization

We have decided to focus our efforts on the detailed surface characterization of the grafted PAA|FTO films and the immobilized **Ru–Cat1** films. The ATR-FTIR spectrum of the plasma treated bare FTO (black line) and the grafted FTO (red line) provide clear evidence of acrylic acid functional groups covalently bound to the grafted FTO and is in agreement with the work of others (Figure 7).[51,52] The broad peak found around 3400 cm^{-1} on the PAA | FTO film is indicative of the –OH stretch found on acrylic acid polymer chains bound to the grafted FTOs (Figure 7). An asymmetric stretching band of C=O found on PAA | FTO appears at 1705 cm^{-1} and then shifts to a lower wavenumber of 1650 cm^{-1} when **Ru–Cat1** was immobilized onto the surface of the grafted FTOs. Aside from the peak shift, the C=O peak associated with acrylic acid decreased significantly as the immobilized FTOs were assembled, also suggesting that immobilization also takes place between the C=O and the anchored **Ru–Cat1** catalyst. The shifting and reduction of chemical peaks associated with the presence of metals found on immobilized surfaces has been studied and is a common occurrence.[52]

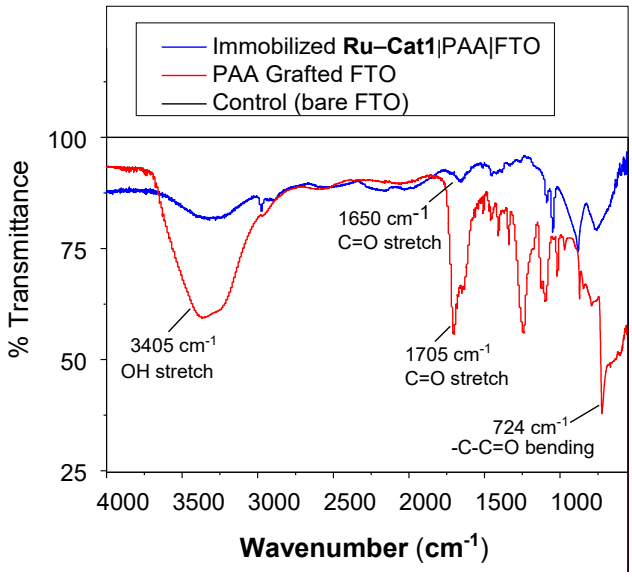

Figure 7. ATR-FTIR spectra of control FTO electrodes treated with argon plasma at 100 watts for 5 minutes (black), acrylic acid grafted onto FTO electrodes (optimal grafting conditions) (red), and immobilized FTO electrodes (optimal immobilization conditions) (blue).

SEM and AFM Characterization

To further characterize PAA|FTO films and Ru immobilized FTO electrodes, AFM images in conjunction with SEM images were taken. As expected, each modification step was accompanied with significant surface topography changes and these changes were visualized using AFM (A) and SEM (B) in Figure 8. When comparing the AFM images of the plasma treated FTO's (Figure $8A_1$ and $8B_1$) to the grafted FTOs (Figure $8A_2$ and $8B_2$), the increase in roughness and thickness of grafted surface is associated with the physical properties of the polymer brush layer. The AFM images of the grafted surface depict a relatively smooth polymer brush layers, with uniform coverage throughout the grafted FTO (Figure $8A_2$ and $8B_2$). The same AFM image was useful in determining the dry polymer brush lengths (435 ± 35 nm), respectively. From this data, the graft density for these particular surfaces was calculated to be 84 μg/cm^2 from the TBO staining. Successfully immobilized FTOs (Figure $8A_3$ and $8B_3$), when compared to the grafted FTOs (Figure $8A_3$ and $8B_3$), demonstrated significant changes in topography (Figure $8A_2$ and $8B_2$). After deposition, the thickness of immobilized layer increased to 970 ± 55 nm. Also, AFM images demonstrate minimal Ru aggregation, with uniform coverage under the above experimental conditions. Corresponding SEM images confirm the results found in AFM imaging, which show uniform and complete coverage with respect to the immobilization of FTOs with **Ru–Cat1**. As expected, SEM images are also in agreement with AFM images,

depicting uniformly and evenly dispersed **Ru–Cat1** immobilization, with very little aggregation (Figure 8).

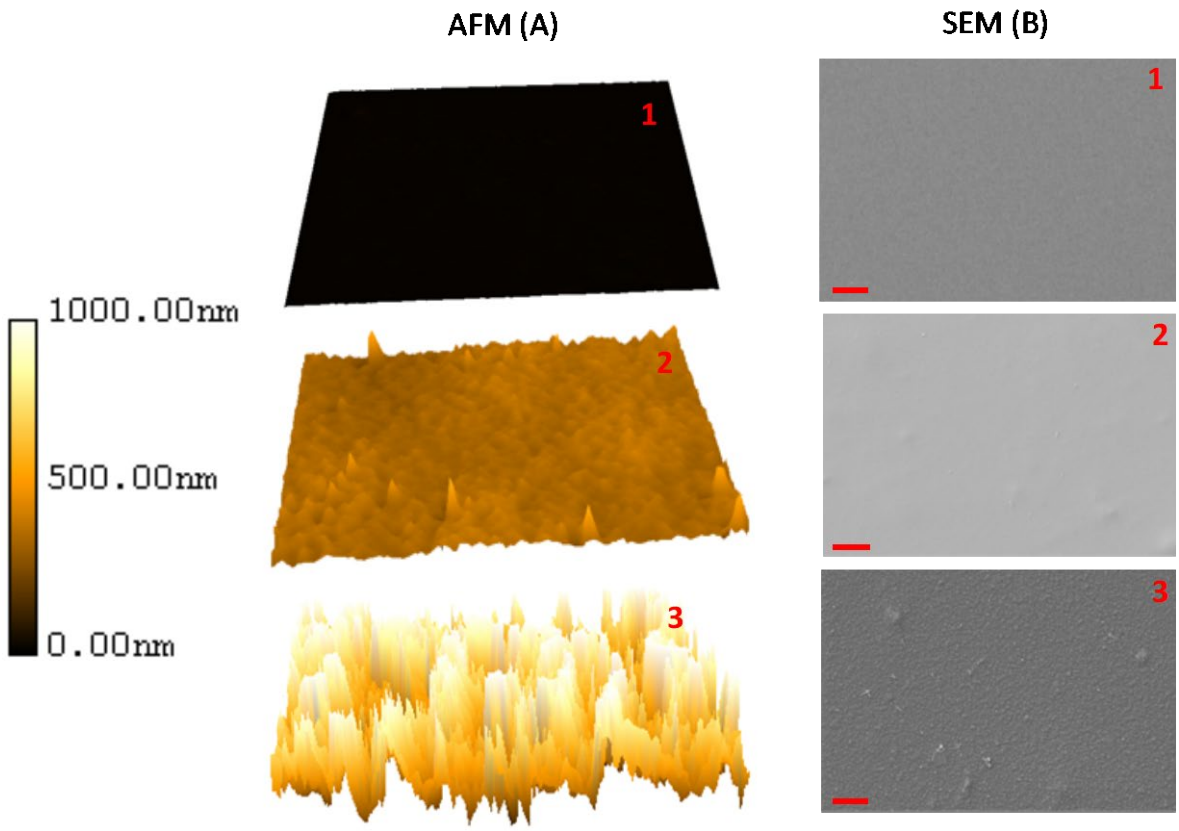

Figure 8. AFM (A), along with corresponding SEM (B) images, of 1) argon plasma treated FTO electrodes (argon plasma at 100 watts for 5 minutes), 2) acrylic acid grafted FTOs (optimal grafting conditions), and 3) **Ru-Cat1** immobilized FTOs (optimal immobilization conditions). Scan distance is 5 µm for AFM images and scale bar is 2 µm for SEM images.

The Effect of pH on Catalytic Water-Oxidation

Upon characterization of the surface of the modified **Ru–Cat1** | PAA | FTO films, we then embarked on investigating the effect of pH on (a) surface redox potential and (b) electrocatatalytic water-oxidation properties. Cyclic voltammetry is a convenient tool for investigating the stability and electro-catalytic activity of the electrodes in sustainable water-oxidation. Figure S7 shows the cyclic voltammograms (CVs) of **Ru–Cat1** | PAA | FTO between pH (2.0–7.2) and noticeably the redox potential ($E_{1/2}$) decreased as the pH of the solution was increased (Table S3). Nevertheless, the plot of $E_{1/2}$ vs. pH in the range between 2–7.3 shows a linear relationship with a slope of –30 mV/pH as shown in Figure S7. In contrast, in solution, the homogenous **Ru–Cat1** catalyst exhibits a Nernstian slope of –59 mV/pH ($1e^-/1H^+$) within pH range (2.0 – 7.0) due to the $[Ru^{III}–OH]^{3+}/[Ru^{II}–OH_2]^{2+}$ couple according to its Pourbaix diagram.[64] In addition, the surface wave in **Ru–Cat1** | PAA | FTO film was pH-independent when the pH ≥ 7; whereas in solution the $[Ru^{III}–OH]^{3+}/[Ru^{II}–OH]^{2+}$ is pH-independent at a higher pH (pH ≥ 10). Our observations are similar to a previously reported study with an encapsulated $[Ru(bpy)_2(py)(H_2O)]^{2+}$ complex (bpy = 2,2’ bipyridine and py = pyridine) in a poly-4-vinylpyridine film coated on a glassy carbon electrode, and the complex showed a pH-independent redox at a low pH ≥ 4.[65] This was attributed to the protonation and deprotonation of free pyridyl groups (pKa = 5.25 in pyridine) in the polymer film which can alter its microstructure and the dielectric properties. This effect was referred to as “pH encapsulation” where the redox properties of the catalyst are dictated by the polymer film and not the pH of the external solution. Similarly, the integration of the **Ru–Cat1** catalyst in a pH-responsive network of grafted PAA capable of accepting or donating protons to the carboxylic group ($RCOO^-$) can also affect the pH environment and thus the redox properties of the attached molecule.[66]

Nevertheless, these types of interactions can be favorable in water-oxidation catalysis, as the carboxyl groups in grafted PAA film can possibly behave as pendant groups and facilitate intramolecular proton transfer. In fact, the second coordination sphere effect due to "pendant carboxyl groups" has been recently shown to greatly enhance catalytic water-oxidation in Ru-carboxylate homogeneous catalysts.[67]

Furthermore, the pH response of the immobilized FTO films with **Ru–Cat1 (**$[Ru^{II}\text{-}OH_2]^{2+}$) was compared to another slide integrated with the **Ru–C3** complex ($[Ru(bpy)_3]^{2+}$). As expected, and based on the CV, the immobilized **Ru–C3** which does not contain a water ligand in its coordination sphere display a pH-independent Ru^{III}/Ru^{II} surface redox couple ($E_{1/2}$ = 1.05 V vs. Ag/AgCl) in acidic (pH ~ 4) and neutral solutions (pH ~ 7) (Figure S6). This clearly affirms that the surface-coupled PCET event observed in the case of **Ru–Cat1**│PAA│FTO and **Ru–Cat2**│PAA│FTO is due to the presence of a water molecule in the Ru(II) coordination sphere $[Ru–OH_2]^{2+}$ when anchored to the grafted polymeric surface (Scheme S2).

Next, we were intrigued to investigate catalytic water-oxidation with our molecular functionalized electrodes. When the potential was cycled to E_{app} of 1.6 V vs. Ag/AgCl to establish the catalytic regime for water-oxidation, we observed a significant enhancement in the current for **Ru–Cat1**|PAA|FTO electrode which was ~ 15 times higher than for the CV recorded for a homogenous aqueous solution of 1.0 mM **Ru–Cat1** at pH 7 using a blank FTO electrode (Figure 5 above). We attribute the larger catalytic currents in the former due the presence of a higher immobilized catalyst loading onto the hydrophilic and conductive grafted PAA polymer brushes layer of FTO. Moreover, the CV of **Ru–Cat1**│PAA│FTO recorded using a scan rate of 0.1 V/s in 0.1 M phosphate buffer solution (pH = 7) showed an enhanced catalytic wave due to water-oxidation as compared to both the grafted PAA|FTO and bare FTO slides (Figure 9). In

that case, the **Ru–Cat1** | PAA | FTO displayed a current density (1000 μA/cm^2) that was an order of magnitude higher than the control bare FTO (100 μA/cm^2) at an applied potential E_{app} of 1.6 V vs. Ag/AgCl. Interestingly, the grafted PAA|FTO (GFTO) exhibits a greater current density than bare FTO at an applied potential of 1.6 V. PAA is a pH-sensitive polyelectrolyte and faster rates of water permeation and charge transport to the bilayer of a grafted PAA surface were observed in neutral and basic pH.[68] However the immobilized **Ru–Cat1** | PAA | FTO exhibited twice as high of catalytic current in comparison to GFTO, and the onset potential favorably shifted from E_{onset} = 1.5 V vs. Ag/AgCl for GFTO to 1.35 V vs. Ag/AgCl for the immobilized catalyst. This is expected as the grafted PAA polymer matrix contains negative charges in aqueous media, which can possibly assist in intramolecular proton transfer between the immobilized catalysts and the grafted surface in water-oxidation catalysis.

Moreover, background subtracted CVs of for **Ru–Cat1** | PAA | FTO at pH 7 in 0.1 M phosphate buffer show that the catalytic current were 5 times higher than in an electrolyte solution with 0.1 M KNO_3 (Figure 10). Also, a noticeable decrease in the onset potential for water-oxidation by a 200 mV in a neutral pH solution of 0.1 M phosphate buffer was observed in comparison to 0.1 M KNO_3 (Figure 10, Table S4). The catalytic water-oxidation waves were pH-dependent, as the background-subtracted current at neutral pH = 7 (in 0.1 M phosphate buffer) were significantly higher (~40 times higher) than at low pH = 1 (in 0.1 M HNO_3) as shown in Figure 10. These results are not surprising as rate enhancement with added buffer bases such as phosphates or hydroxide (OH^-) is consistent with the base-assisted O–O bond formation pathway as previously reported by Meyer and co-workers (Figure 11).[32,69] Chronoamperometry measurements were further performed to test the activity and stability of **Ru–Cat1**|PAA|FTO. Figure 9 shows the chronoamperogram of **Ru–Cat1**|PAA|FTO at pH 7 (0.1 M phosphate buffer,

ionic strength = 0.1 M) in comparison to bare FTO recorded at an applied potential E_{app} = 1.5 V vs. Ag/AgCl for 1 h. After monitoring for this long-term period, sustained catalytic current were obtained for the **Ru–Cat1**|PAA|FTO (~105 mA cm^{-2}) at pH 7 in comparison with the control experiment with bare FTO (Figure 9). A turnover frequency (TOF) of 0.20 s^{-1} was calculated based on equation S1 and more details can be found in the supporting information.

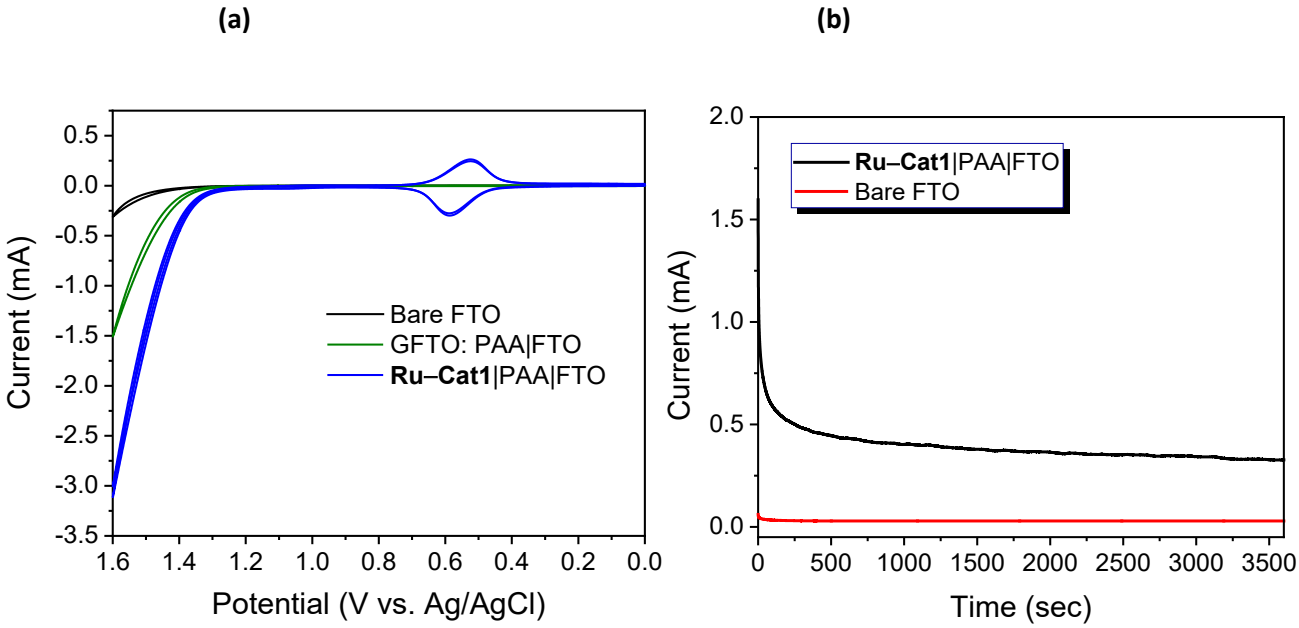

Figure 9. (a) Cyclic voltammogram (CV) of bare FTO (black), GFTO: grafted PAA|FTO (green) and immobilized **Ru–Cat1**|PAA|FTO (blue) in 0.1 M phosphate buffer at pH 7. The measurements were performed by scanning 4 consecutive segments from 0 V to 1.6 V vs. Ag/AgCl at a scan rate of 0.1 V/s. (b) Chronoamperometric responses of **Ru–Cat1**|PAA|FTO (black) and bare FTO (red) at an applied potential E_{app} = 1.5 V (vs. Ag/AgCl) in 0.1 M phosphate buffer adjusted to pH = 7 (ionic strength 0.1 M).

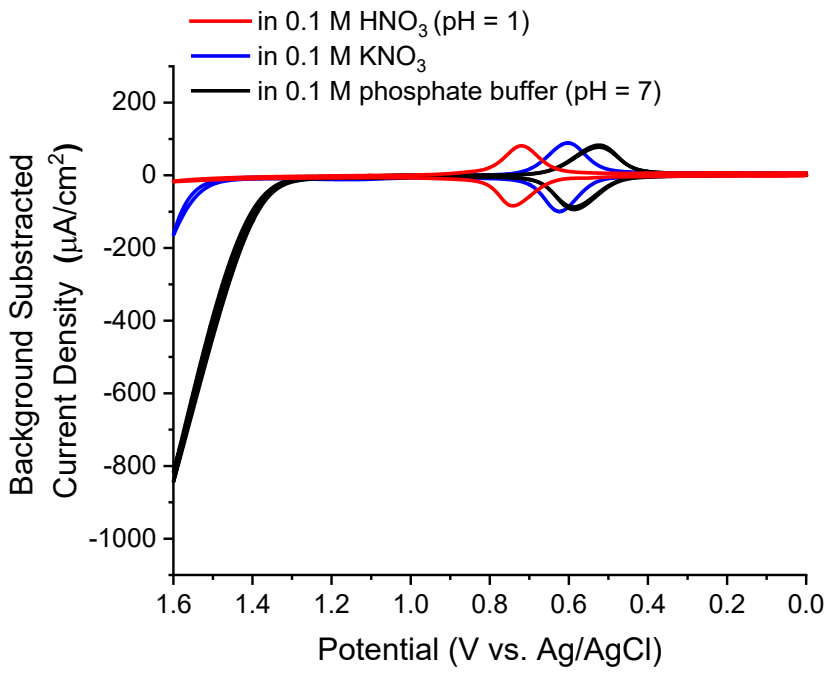

Figure 10. Background subtracted cyclic voltammograms of **Ru–Cat1** | PAA | FTO in 0.1 M phosphate buffer at pH = 7 (black) and 0.1 M KNO_3 (blue) and 0.1 M HNO_3 (red) at a scan rate 100 mV s^{-1}.

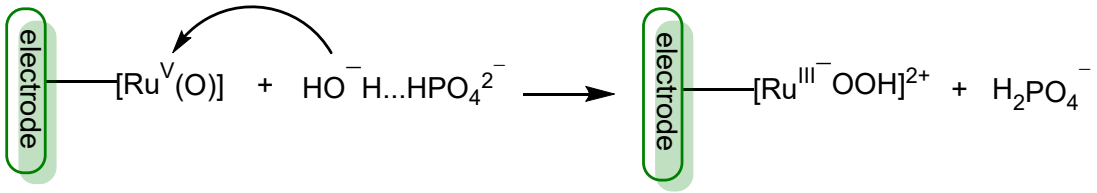

Figure 11. Proposed base-assisted water-oxidation mechanism for the immobilized catalysts **Ru–Cat1** and **Ru–Cat2** on grafted PAA|FTO.

Finally, we tested the electrochemical stability of the immobilized **Ru–Cat1** film at pH = 1 (in 0.1 M HNO_3). Similarly, the CV of the film at pH 1 shows a collapsed reversible Ru^{IV}/Ru^{III} and Ru^{III}/Ru^{II} as observed at pH = 7. The current density remained steady at pH = 1 after performing several consecutive scans which indicates the relative stability of the complex on the surface at low pH. However, upon leaving the slide for prolonged hours (~4 h) in 0.1 M HNO_3 electrolyte solution, a 95±4% significant decrease in surface coverage was observed along with an observable change in the color of the acidic solution to orange due to the leaching of the **Ru–Cat1**, as confirmed by UV-visible spectral analysis. This is not surprising as the surface loss of the catalyst is induced by the protonation of the negatively charged carboxyl group of PAA at low pH. Nevertheless, the rate of desorption of the catalyst from the grafted PAA the surface appears to be slow (95% loss in 4 h). Moreover, when the desorbed PAA|FTO film was removed from the acid solution and re-submerged for few hours (~2 h) in an aqueous solution containing a neutral aqueous solution of 1 mM **Ru–Cat1**, we find that the catalyst **Ru–Cat1** can be reloaded to the PAA|FTO film. The final surface coverage measured after ca. 4 h of re-soaking the slides were comparable to those of freshly prepared grafted PAA slides soaked during the same period (Figure S9). Thus the network of grafted PAA brushes onto FTO provides a flexible substrate platform which can immobilize or release the molecular catalyst by simply tuning the pH of the solution.

CONCLUSION

In this work, argon plasma-induced graft polymerization of polyacryclic acid (PAA) films onto the FTO conductive glass were constructed as a robust platform for the immobilization of molecular water-oxidation catalysts (WOCs). When generated under optimal grafting conditions,

the “Grafting-From” approach resulted in complete grafting coverage, with uniformly and evenly dispersed PAA grafted FTO electrodes. Electrochemical characterization, contact angle (supplementary information), SEM, AFM, IR data all provided quantitative and qualitative information about the nature of the immobilized plasma grafted FTO films. Ru(II) non-derivatized benchmark WOCs (**Ru–Cat1** and **Ru–Cat2**) and the chromophore **Ru–C3** were directly immobilized to the surface modified FTO slides without the need of synthetic modification of the molecular complex. The PAA grafted layer provides a stable environment for binding of the oxidized immobilized Ru(II) complexes. Significant enhancement in water-oxidation catalytic currents were observed in 0.1 M phosphate buffer at pH 6–7 as compared to low pH or aqueous solutions containing 0.1 M KNO_3 which indicates a base-assisted PCET process. Electrochemical PCET behavior was observed for **Ru–Cat1** and **Ru–Cat2** and indicated the presence of water ligand in the coordination sphere when immobilized on the grafted polymer. Based on our results, we believe that the enhanced surface stability upon oxidation for **Ru–Cat1** and **Ru–Cat2** in comparison to **Ru–C3** at pH = 7 is due to synergistic effects arising from the grafted cross-linked network of PAA polymer brushes and H-bonding that can ensue between the negatively charged carboxyl functional groups of the PAA film and the water coordinated ligand in the immobilized complex $[Ru^{II}\text{-}OH_2]^{2+}$. Furthermore, our findings demonstrate that the plasma-grafted polymeric network provides as a flexible substrate platform to immobilize or release the molecular catalyst by simply tuning the pH of the solution. To the best of our knowledge, this is the first example of Ru(II) molecular water-oxidation catalysts anchored to a plasma-assisted grafted polymer brushes on conductive FTO glass. This methodology offers a simple and a practical surface modification strategy to directly anchor

unmodified homogeneous water-oxidation catalysts onto conductive surfaces and has the potential to increase the scope of WOCs hybrid composites.

ASSOCIATED CONTENT

Supporting Information.

Electrochemical and contact angle (Contact angle (CA) measurements are discussed and additional electrochemical data are given in Figure S1–S9 and Tables S1–S4. This material is available free of charge via the Internet at http://pubs.acs.org.

AUTHOR INFORMATION

Corresponding Author

†Email: ybadiei@saintpeters.edu;

§ Email: ctraba@fdu.edu.

Notes

The authors declare no competing financial interest.

ACKNOWLEDGEMENTS

The majority of the work was carried out at Saint Peter's University and was financially supported by the George J. Hilsdorf, S.J. Endowment Fund and the United States Department of Education DOED [SURGE grant #PO31C160038]. Y.M.B. was awarded the Kenny Fellowship 2020 from SPU. C.A. was awarded the Independent College Fund of New Jersey (ICFNJ) private research grant in 2019. The work carried out at Brookhaven National Laboratory was

supported by the U.S. Department of Energy, Office of Science, Division of Chemical Sciences, Geosciences, & Biosciences, Office of Basic Energy Sciences under contract DE-SC0012704.

REFERENCES

(1) Lewis, N. S.; Nocera, D. G. Powering the planet: Chemical challenges in solar energy utilization. *Proc. Natl. Acad. Sci. U.S.A.* **2006**, *103*, 15729−15735.

(2) Nocera, D. G. Solar Fuels and Solar Chemicals Industry. *Acc. Chem. Res.* **2017**, *50*, 616-619.

(3) Barber, J. Photosynthetic energy conversion: natural and artificial. *Chem. Soc. Rev.* **2009**, *38*, 185-196.

(4) Materna, K. L.; Crabtree, R. H.; Brudvig, G. W. Anchoring groups for photocatalytic water oxidation on metal oxide surfaces. *Chem. Soc. Rev.* **2017**, *46*, 6099-6110.

(5) Turner, J. A. Sustainable Hydrogen Production. *Science* **2004**, *305*, 972.

(6) Tong, L.; Thummel, R. P. Mononuclear ruthenium polypyridine complexes that catalyze water oxidation. *Chem. Sci.* **2016**, *7*, 6591-6603.

(7) Blakemore, J. D.; Crabtree, R. H.; Brudvig, G. W. Molecular Catalysts for Water Oxidation. *Chem. Rev.* **2015**, *115*, 12974-13005.

(8) Yano, J.; Kern, J.; Sauer, K.; Latimer, M. J.; Pushkar, Y.; Biesiadka, J.; Loll, B.; Saenger, W.; Messinger, J.; Zouni, A.; Yachandra, V. K. Where Water Is Oxidized to Dioxygen: Structure of the Photosynthetic Mn4Ca Cluster. *Science* **2006**, *314*, 821.

(9) Cady, C. W.; Crabtree, R. H.; Brudvig, G. W. Functional models for the oxygen-evolving complex of photosystem II. *Coord. Chem. Rev.* **2008**, *252*, 444-455.

(10) Brimblecombe, R.; Koo, A.; Dismukes, G. C.; Swiegers, G. F.; Spiccia, L. Solar Driven Water Oxidation by a Bioinspired Manganese Molecular Catalyst. *J. Am. Chem. Soc.* **2010**, *132*, 2892-2894.

(11) Concepcion, J. J.; Jurss, J. W.; Brennaman, M. K.; Hoertz, P. G.; Patrocinio, A. O. T.; Iha, N. Y. M.; Templeton, J. L.; Meyer, T. J. Making Oxygen with Ruthenium Complexes. *Acc. Chem. Res.* **2009**, *42*, 1954-1965.

(12) Limburg, B.; Bouwman, E.; Bonnet, S. Molecular water oxidation catalysts based on transition metals and their decomposition pathways. *Coord. Chem. Rev.* **2012**, *256*, 1451-1467.

(13) Gersten, S. W.; Samuels, G. J.; Meyer, T. J. Catalytic-Oxidation of Water by an Oxo-Bridged Ruthenium Dimer. *J. Am. Chem. Soc.* **1982**, *104*, 4029-4030.

(14) Wasylenko, D. J.; Palmer, R. D.; Berlinguette, C. P. Homogeneous water oxidation catalysts containing a single metal site. *Chem. Comm.* **2013**, *49*, 218-227.

(15) Duan, L.; Bozoglian, F.; Mandal, S.; Stewart, B.; Privalov, T.; Llobet, A.; Sun, L. A molecular ruthenium catalyst with water-oxidation activity comparable to that of photosystem II. *Nat. Chem.* **2012**, *4*, 418-423.

(16) Codolà, Z.; João, M. S. C.; Royo, B.; Costas, M.; Lloret-Fillol, J. Highly Effective Water Oxidation Catalysis with Iridium Complexes through the Use of NaIO4. *Chem. Eur. J.* **2013**, *19*, 7203-7213.

(17) Hull, J. F.; Balcells, D.; Blakemore, J. D.; Incarvito, C. D.; Eisenstein, O.; Brudvig, G. W.; Crabtree, R. H. Highly Active and Robust Cp* Iridium Complexes for Catalytic Water Oxidation. *J. Am. Chem. Soc.* **2009**, *131*, 8730-+.

(18) Moore, G. F.; Blakemore, J. D.; Milot, R. L.; Hull, J. F.; Song, H. E.; Cai, L.; Schmuttenmaer, C. A.; Crabtree, R. H.; Brudvig, G. W. A visible light water-splitting cell with a photoanode formed by codeposition of a high-potential porphyrin and an iridium water-oxidation catalyst. *Energy Environ. Sci.* **2011**, *4*, 2389-2392.

(19) Badiei, Y. M.; Xie, Y.; Renderos, G.; Concepcion, J. J.; Szalda, D.; Guevara, J.; Rosales, R.; Ortiz, E.; Hankins, M. Rapid identification of homogeneous O2 evolution catalysts and comparative studies of Ru(II)-carboxamides vs. Ru(II)-carboxylates in water-oxidation. *J. Catal.* **2019**, *369*, 10-20.

(20) Shaffer, D. W.; Xie, Y.; Concepcion, J. J. O–O bond formation in ruthenium-catalyzed water oxidation: single-site nucleophilic attack vs. O–O radical coupling. *Chem. Soc. Rev.* **2017**, *46*, 6170-6193.

(21) Tseng, H. W.; Zong, R.; Muckerman, J. T.; Thummel, R. Mononuclear Ruthenium(II) Complexes That Catalyze Water Oxidation. *Inorg. Chem.* **2008**, *47*, 11763-11773.

(22) Concepcion, J. J.; Jurss, J. W.; Norris, M. R.; Chen, Z. F.; Templeton, J. L.; Meyer, T. J. Catalytic Water Oxidation by Single-Site Ruthenium Catalysts. *Inorg. Chem.* **2010**, *49*, 1277-1279.

(23) Kumar, A.; S, S.; Varshney, P.; Paul, A.; Jeyaraman, S. Aminophenyl-substituted cobalt(iii) corrole: a bifunctional electrocatalyst for the oxygen and hydrogen evolution reactions. *Dalton Transactions* **2019**, *48*, 11345-11351.

(24) Kanan, M. W.; Nocera, D. G. In situ formation of an oxygen-evolving catalyst in neutral water containing phosphate and Co2+. *Science* **2008**, *321*, 1072-1075.

(25) Dogutan, D. K.; Stoian, S. A.; McGuire, R.; Schwalbe, M.; Teets, T. S.; Nocera, D. G. Hangman Corroles: Efficient Synthesis and Oxygen Reaction Chemistry. *J. Am. Chem. Soc.* **2011**, *133*, 131-140.

(26) Fillol, J. L.; Codolà, Z.; Garcia-Bosch, I.; Gómez, L.; Pla, J. J.; Costas, M. Efficient water oxidation catalysts based on readily available iron coordination complexes. *Nat. Chem.* **2011**, *3*, 807-813.

(27) Ellis, W. C.; McDaniel, N. D.; Bernhard, S.; Collins, T. J. Fast Water Oxidation Using Iron. *J. Am. Chem. Soc.* **2010**, *132*, 10990-10991.

(28) Garrido-Barros, P.; Grau, S.; Drouet, S.; Benet-Buchholz, J.; Gimbert-Suriñach, C.; Llobet, A. Can Ni Complexes Behave as Molecular Water Oxidation Catalysts? *ACS Catal.* **2019**, *9*, 3936-3945.

(29) Wang, L.; Duan, L.; Ambre, R. B.; Daniel, Q.; Chen, H.; Sun, J.; Das, B.; Thapper, A.; Uhlig, J.; Dinér, P.; Sun, L. A nickel (II) PY5 complex as an electrocatalyst for water oxidation. *J. Catal.* **2016**, *335*, 72-78.

(30) Barnett, S. M.; Goldberg, K. I.; Mayer, J. M. A soluble copper–bipyridine water-oxidation electrocatalyst. *Nat. Chem.* **2012**, *4*, 498-502.

(31) Du, J., Chen, Z., Ye, S., Wiley, B. J. and Meyer, T. J. Copper as a Robust and Transparent Electrocatalyst for Water Oxidation. *Angew. Chem. Int. Ed.* **2015**, *54*, 2073–2078.

(32) Chen, Z.; Concepcion, J. J.; Jurss, J. W.; Meyer, T. J. Single-Site, Catalytic Water Oxidation on Oxide Surfaces. *J. Am. Chem. Soc.* **2009**, *131*, 15580-15581.

(33) Wasylenko, D. J.; Ganesamoorthy, C.; Koivisto, B. D.; Henderson, M. A.; Berlinguette, C. P. Insight into Water Oxidation by Mononuclear Polypyridyl Ru Catalysts. *Inorg. Chem.* **2010**, *49*, 2202-2209.

(34) Duan, L.; Wang, L.; Li, F.; Li, F.; Sun, L. Highly Efficient Bioinspired Molecular Ru Water Oxidation Catalysts with Negatively Charged Backbone Ligands. *Acc. Chem. Res.* **2015**, *48*, 2084-2096.

(35) Muckerman, J. T.; Kowalczyk, M.; Badiei, Y. M.; Polyansky, D. E.; Concepcion, J. J.; Zong, R.; Thummel, R. P.; Fujita, E. New Water Oxidation Chemistry of a Seven-Coordinate Ruthenium Complex with a Tetradentate Polypyridyl Ligand. *Inorganic Chemistry* **2014**, *53*, 6904-6913.

(36) Badiei, Y. M.; Polyansky, D. E.; Muckerman, J. T.; Szalda, D. J.; Haberdar, R.; Zong, R.; Thummel, R. P.; Fujita, E. Water Oxidation with Mononuclear Ruthenium(II) Polypyridine Complexes Involving a Direct RuIV═O Pathway in Neutral and Alkaline Media. *Inorg. Chem.* **2013**, *52*, 8845-8850.

(37) Huynh, M. H. V.; Meyer, T. J. Proton-Coupled Electron Transfer. *Chem. Rev.* **2007**, *107*, 5004-5064.

(38) Weinberg, D. R.; Gagliardi, C. J.; Hull, J. F.; Murphy, C. F.; Kent, C. A.; Westlake, B. C.; Paul, A.; Ess, D. H.; McCafferty, D. G.; Meyer, T. J. Proton-Coupled Electron Transfer. *Chem. Rev.* **2012**, *112*, 4016-4093.

(39) Concepcion, J. J.; Tsai, M. K.; Muckerman, J. T.; Meyer, T. J. Mechanism of Water Oxidation by Single-Site Ruthenium Complex Catalysts. *J. Am. Chem. Soc.* **2010**, *132*, 1545-1557.

(40) Li, F.; Yang, H.; Li, W.; Sun, L. Device Fabrication for Water Oxidation, Hydrogen Generation, and CO2 Reduction via Molecular Engineering. *Joule* **2018**, *2*, 36-60.

(41) Bullock, R. M.; Das, A. K.; Appel, A. M. Surface Immobilization of Molecular Electrocatalysts for Energy Conversion. *Chem. Eur. J.* **2017**, *23*, 7626-7641.

(42) Zahran, Z. N.; Tsubonouchi, Y.; Mohamed, E. A.; Yagi, M. Recent Advances in the Development of Molecular Catalyst-Based Anodes for Water Oxidation toward Artificial Photosynthesis. *ChemSusChem* **2019**, *12*, 1775-1793.

(43) Young, K. J.; Martini, L. A.; Milot, R. L.; Snoeberger, R. C.; Batista, V. S.; Schmuttenmaer, C. A.; Crabtree, R. H.; Brudvig, G. W. Light-driven water oxidation for solar fuels. *Coord. Chem. Rev.* **2012**, *256*, 2503-2520.

(44) Rosser, T. E.; Reisner, E. Understanding Immobilized Molecular Catalysts for Fuel-Forming Reactions through UV/Vis Spectroelectrochemistry. *ACS Catal.* **2017**, *7*, 3131-3141.

(45) Concepcion, J. J.; Zhong, D. K.; Szalda, D. J.; Muckerman, J. T.; Fujita, E. Mechanism of water oxidation by Ru(bda)(L)(2) : the return of the "blue dimer". *Chem. Comm.* **2015**, *51*, 4105-4108.

(46) Zhong, D. K.; Zhao, S.; Polyansky, D. E.; Fujita, E. Diminished photoisomerization of active ruthenium water oxidation catalyst by anchoring to metal oxide electrodes. *J. Catal.* **2013**, *307*, 140-147.

(47) Hyde, J. T.; Hanson, K.; Vannucci, A. K.; Lapides, A. M.; Alibabaei, L.; Norris, M. R.; Meyer, T. J.; Harrison, D. P. Electrochemical Instability of Phosphonate-Derivatized, Ruthenium(III) Polypyridyl Complexes on Metal Oxide Surfaces. *ACS Appl. Mater. Interfaces* **2015**, *7*, 9554-9562.

(48) Wu, L.; Nayak, A.; Shao, J.; Meyer, T. J. Crossing the bridge from molecular catalysis to a heterogenous electrode in electrocatalytic water oxidation. *Proc. Natl. Acad. Sci. U.S.A.* **2019**, *116*, 11153.

(49) Wadsworth, B. L.; Beiler, A. M.; Khusnutdinova, D.; Jacob, S. I.; Moore, G. F. Electrocatalytic and Optical Properties of Cobaloxime Catalysts Immobilized at a Surface-Grafted Polymer Interface. *ACS Catal.* **2016**, *6*, 8048-8057.

(50) Wang, L.; Polyansky, D. E.; Concepcion, J. J. Self-Assembled Bilayers as an Anchoring Strategy: Catalysts, Chromophores, and Chromophore-Catalyst Assemblies. *J. Am. Chem. Soc.* **2019**, *141*, 8020-8024.

(51) Ambi, A.; Vera, C.; Parikh, N.; Perez, N.; Lopez Rojas, A.; Kumar, S.; Stradford, C.; Borbon, K.; Bryan, J.; Traba, C. Plasma-initiated graft polymerization as an immobilization platform for metal free Russian propolis ethanol extracts designed specifically for biomaterials. *Biofouling* **2018**, *34*, 557-568.

(52) Ambi, A.; Parikh, N.; Vera, C.; Burns, K.; Montano, N.; Sciorra, L.; Epstein, J.; Zeng, D.; Traba, C. Anti-infection silver nanoparticle immobilized biomaterials facilitated by argon plasma grafting technology. *Biofouling* **2018**, *34*, 273-286.

(53) Polidor, D.; Brito, G.; Roca, J.; Sciorra, L.; Li, C.; Traba, C. Can the argon plasma "Grafting-From" approach be used for the modification of nanoparticle systems? *Colloids Interface Sci. Commun.* **2020**, *37*, 100269.

(54) Renderos, G.; Aquino, T.; Gutierrez, K.; Badiei, Y. M. Facile Method To Study Catalytic Oxygen Evolution Using a Dissolved Oxygen Optical Probe: An Undergraduate Chemistry Laboratory To Appreciate Artificial Photosynthesis. *J. Chem. Ed.* **2017**, *94*, 922-927.

(55) You, S.-J.; Semblante, G. U.; Lu, S.-C.; Damodar, R. A.; Wei, T.-C. Evaluation of the antifouling and photocatalytic properties of poly(vinylidene fluoride) plasma-grafted poly(acrylic acid) membrane with self-assembled TiO2. *J. Hazard. Mater* **2012**, *237-238*, 10-19.

(56) Dou, S.; Tao, L.; Wang, R.; El Hankari, S.; Chen, R.; Wang, S. Plasma-Assisted Synthesis and Surface Modification of Electrode Materials for Renewable Energy. *Adv. Mater.* **2018**, *30*, 1705850.

(57) Gupta, B.; Anjum, N. In *Radiation Effects on Polymers for Biological Use*; Kausch, H., Anjum, N., Chevolot, Y., Gupta, B., Léonard, D., Mathieu, H. J., Pruitt, L. A., Ruiz-Taylor, L., Scholz, M., Eds.; Springer Berlin Heidelberg: Berlin, Heidelberg, 2003, p 35-61.

(58) Luo, Y.; Cheng, R.; Shen, J.; Chen, X.; Lu, Z.; Chen, Y.; Sun, Z.; Huang, S. Plasma-modified SnO2:F substrate for efficient cobalt selenide counter in dye sensitized solar cell. *RSC Adv.* **2014**, *4*, 44896-44901.

(59) Conrads, H.; Schmidt, M. Plasma generation and plasma sources. *Plasma Sources Sci. Technol.* **2000**, *9*, 441-454.

(60) Wadsworth, B. L.; Khusnutdinova, D.; Moore, G. F. Polymeric coatings for applications in electrocatalytic and photoelectrosynthetic fuel production. *J. Mater. Chem. A* **2018**, *6*, 21654-21665.

(61) Leem, G.; Sherman, B. D.; Schanze, K. S. Polymer-based chromophore–catalyst assemblies for solar energy conversion. *Nano Converg.* **2017**, *4*, 37.

(62) Bard, A. J. F., L. R. *Electrochemical Methods: Fundamentals and Applications*; 2nd ed. ed.; Wiley Global Education: New York, 2001.

(63) Hyde, J. T.; Hanson, K.; Vannucci, A. K.; Lapides, A. M.; Alibabaei, L.; Norris, M. R.; Meyer, T. J.; Harrison, D. P. Electrochemical Instability of Phosphonate-Derivatized, Ruthenium(III) Polypyridyl Complexes on Metal Oxide Surfaces. *ACS Appl. Mater. Interfaces* **2015**, *7*, 9554-9562.

(64) Takeuchi, K. J.; Thompson, M. S.; Pipes, D. W.; Meyer, T. J. Redox and spectral properties of monooxo polypyridyl complexes of ruthenium and osmium in aqueous media. *Inorg. Chem.* **1984**, *23*, 1845-1851.

(65) Samuels, G. J.; Meyer, T. J. An electrode-supported oxidation catalyst based on ruthenium(IV). pH "encapsulation" in a polymer film. *J. Am. Chem. Soc.* **1981**, *103*, 307-312.

(66) Liu, F.; Urban, M. W. Recent advances and challenges in designing stimuli-responsive polymers. *Prog. Polym. Sci.* **2010**, *35*, 3-23.

(67) Vereshchuk, N.; Matheu, R.; Benet-Buchholz, J.; Pipelier, M.; Lebreton, J.; Dubreuil, D.; Tessier, A.; Gimbert-Suriñach, C.; Ertem, M. Z.; Llobet, A. Second Coordination Sphere Effects in an Evolved Ru Complex Based on Highly Adaptable Ligand Results in Rapid Water Oxidation Catalysis. *J. Am. Chem. Soc.* **2020**, *142*, 5068-5077.

(68) Cao, P.-F.; Mangadlao, J. D.; Advincula, R. C. Stimuli-Responsive Polymers and their Potential Applications in Oil-Gas Industry. *Polym. Rev.* **2015**, *55*, 706-733.

(69) Chen, Z. F.; Concepcion, J. J.; Hu, X. Q.; Yang, W. T.; Hoertz, P. G.; Meyer, T. J. Concerted O atom-proton transfer in the O-O bond forming step in water oxidation. *Proc. Natl. Acad. Sci. U.S.A.* **2010**, *107*, 7225-7229.